AAPS PharmSciTech (2019) 20: 316
DOI: 10.1208/s12249-019-1449-1

Check for updates

Research Article

A Lipid Micellar System Loaded with Dexamethasone Palmitate Alleviates Rheumatoid Arthritis

Xinxin Wang,[1] Yan Feng,[2] Jijun Fu,[3] Cuishuan Wu,[4] Bing He,[2] Hua Zhang,[2] Xueqing Wang,[2] Wenbing Dai,[2] Yong Sun,[1] and Qiang Zhang[2,5]

Received 16 April 2019; accepted 1 June 2019; published online 10 October 2019

Abstract. Glucocorticoids have been confirmed to be effective in the treatment of a variety of inflammatory diseases. However, their application encounters limitations in terms of tissue distribution and bioavailability *in vivo*. To address these key issues, we designed and developed a nanopreparation by using egg yolk lecithin/sodium glycocholate (EYL/SGC) and utilize such mixed micelles (MMs) to encapsulate dexamethasone palmitate (DMP) for the treatment of rheumatoid arthritis (RA). The prepared DMP-MMs had an average particle size of 49.18 ± 0.43 nm and were compared with an emulsion-based dexamethasone palmitate. Pharmacokinetic and *in vivo* fluorescence imaging showed that mixed micelles had higher bioavailability and targeting efficiency in inflammatory sites. An arthritis rat model was established *via* induction by Complete Freund's Adjuvant (CFA), followed by the efficacy studies by the observations of paw volume, histology, spleen index, pro-inflammatory cytokines, and CT images. It was confirmed that intravenous injection of DMP-MMs exhibited advantages in alleviating joint inflammation compared with the emulsion system. Composed of pharmaceutical adjuvants only, the nanoscale mixed micelles seem a promising carrier system for the RA treatment with lipophilic drugs.

KEY WORDS: mixed micelles; nanomedicine; passive targeting; dexamethasone palmitate; rheumatoid arthritis.

INTRODUCTION

Rheumatoid arthritis (RA), a chronic inflammatory disorder, afflicts approximately 1% of the population worldwide (1). Its mainly pathological symptom is synovial hyperplasia. Over-proliferated synovial cells together with inflammatory cells and small blood vessels form pannus and cover the cartilage surface, and finally block the nutrient supply. Moreover, the over-proliferated cells secrete a variety of proteases, collagenases, *etc.*, which would degrade cartilage and bone, eventually leading to loss of joint function. The inflammatory environment in the synovial cavity is regulated by complex cytokines and chemokine networks. For example, macrophages overexpress inflammatory factors, including tumor necrosis factor-α (TNF-α), interleukin-1β (IL-1β), and interleukin-6 (IL-6) (2–4).

Although RA is far from being completely cured at present, pharmacotherapy could prevent its progression. Glucocorticoids (GCs) play an irreplaceable role in the treatment of RA because they enable rapid alleviation of joint swelling and joint damage (5–7). GCs exert anti-inflammatory effects through a variety of mechanisms (8,9). Meanwhile, due to the multi-target effect of GCs, a variety of adverse effects have been reported after its systemic administration, such as weight loss and high blood sugar (10). Therefore, it is urgent to improve the safety of GC treatment and the life quality of RA patients.

Due to the leaky vessels in tumors, the nanoparticles selectively accumulate in the malignant tissues; the phenomenon is well known as enhanced permeability and retention (EPR) effects (11–14). This strategy also applies to the RA treatment. Studies show that the vascular permeability in the inflammation site of RA was enhanced due to the leaky vascular networks (15). Actually, the therapeutic effects of some nanoformulations on RA have been confirmed (16–19). In addition, lecithin-based nanoparticles could enhance the oral bioavailability of hydrophobic drugs and improve their anti-inflammatory activity (20,21).

[1] Department of Pharmaceutics, School of Pharmacy, Qingdao University, Qingdao, 266021, China.
[2] Beijing Key Laboratory of Molecular Pharmaceutics and New Drug Delivery Systems, School of Pharmaceutical Sciences, Peking University, Beijing, 100191, China.
[3] School of Pharmaceutical Science, Guangzhou Medical University, Guangzhou, 511436, China.
[4] Beijing Delivery Pharmaceutical Technology Co., Ltd, Beijing, China.
[5] To whom correspondence should be addressed. (e–mail: zqdodo@bjmu.edu.cn)

It was demonstrated that the nanoparticles bigger than 200 nm were easily eliminated from the circulation system by liver and spleen (22), and small nanoparticles (less than 10 nm) were quickly excreted through the urine. As a result, moderate particle size is necessary to realize the long circulation of the nanoparticles and finally guarantee the satisfying accumulation in the synovial cavity. From this aspect, despite the extensive employment of the micron emulsions for insoluble drugs, it is not a suitable vector for RA treatment as its size is approximately 200 nm. Micelles exhibit moderate particle size of about 100 nm for RA treatment. Mixed micelles may be a better system with EPR effect. It has smaller particle size, good stability *in vivo*, and simple preparation compared with the existing marketed preparations, especially emulsions.

Egg yolk lecithin and sodium glycocholate are frequently employed in micron emulsions and have good physiological compatibility and safety (23,24). In this project, these two materials are used to prepare the mixed micelles. Dexamethasone palmitate, a derivative of dexamethasone, was loaded in the center of mixed micelles. Despite similar components, the mixed micelles was supposed to show smaller particle size than the commercially available emulsion Limethason® (25). In the RA rat model, the therapeutic effect of the micelles on chronic RA is evaluated by the paw volume, pathological examination, spleen index, and pro-inflammatory factor. We also studied the preventive effect of the drug delivery system in the acute inflammation model. Furthermore, the pharmacokinetics and biodistribution were also investigated.

MATERIALS AND METHODS

Materials

Egg yolk lecithin (PL-100M) was obtained from Kewpie Corporation (Japan). Glycocholic acid was purchased from Aladdin (Shanghai, China). Dexamethasone palmitate was purchased from Hekang Pharmaceutical Co., Ltd. (Henan, China). Complete Freund's adjuvant (10 mg/mL of the heat-killed *Mycobacterium*) was purchased from Chondrex (Washington DC, USA). Carrageenan was purchased from Sigma-Aldrich Chemical Co. (Missouri, USA). The near-infrared fluorescence dye Dir was purchased from Biorj (Beijing, China).

Animals

Male Sprague-Dawley rats (180 ± 20 g) were purchased from Beijing Vital River Laboratory Animal Technology. Rats were housed and fed in specific pathogen-free environment in the animal facility of the School of Peking University Health Science Center. All animal studies conformed to the guidelines of care and use of laboratory animals of Institutional Animal Care and Use Committee of Peking University.

Preparation of DMP-MMs

We prepared DMP-MMs as a previously reported method (26). Briefly, DMP, EYL, NaOH, and glycocholic acid were dissolved in 8 mL of anhydrous ethanol by ultrasonication. Then, the solution was evaporated at 40°C with a rotating evaporator (SHZ-DIII; Yuhua Tech, China). We obtained a thin film of drug-carrier materials. The film was immediately hydrated in 5 mL of deionized water for 5 min *via* ultrasound (KQ-100DE; Kunshan Tech, China). The micellar solution was centrifuged at 12,000 rpm for 10 min to remove un-encapsulated drug. The DMP-MMs existed in the supernatant.

The Dir-loaded mixed micelles (Dir-MMs) were prepared according to the above methods. The Dir emulsion with the same prescription as Limethason® (Dir-EL) was prepared by probe ultrasonic (SCIENTZ-IID; Xinzhi Tech, China) method as previously described (27).

Characterization of DMP-MMs

The diameter, distribution, and zeta potential were measured in triplicates by dynamic light scattering (DLS; Malvern, UK) at 25°C. Transmission electron microscope (TEM; JEM1200EX, Japan) and atomic force microscope (AFM; Dimension Icon, USA) were used to confirm the surface morphology of DMP-MMs.

The concentration of the DMP encapsulated in micelles was determined using high-performance liquid chromatography (HPLC; Shimadzu Tech, Japan) using an RP-18e–5 μm column (250 mm × 4.6 mm). The micellar solution was diluted 100 times with methanol, and 20 μL was injected into the HPLC. The detection wavelength of DMP was 240 nm. The mobile phase consists of methanol and water with a volume ratio of 95:5. The flow rate was set at 1.0 ml/min with column temperature of 37°C. The formulas for calculating entrapment efficiency (EE%) and drug loading (DL%) are as follows:

$$\mathrm{EE\%} = \left(M_{\mathrm{dmp}}/M_{\mathrm{dmp\ added}}\right) \times 100\%$$

$$\mathrm{DL\%} = \left(M_{\mathrm{dmp}}/M_{\mathrm{dmp}} + M_{\mathrm{ingredients}}\right) \times 100\%$$

where M_{dmp} is the weight of the loaded (solubilized) DMP and $M_{\mathrm{ingredients}}$ are carrier material in the micellar solution, while $M_{\mathrm{dmp\ added}}$ is the weight of the DMP originally added to the prescription.

Critical Micelle Concentration (CMC)

The CMC of EPC-SGC-MMs in deionized water was confirmed using pyrene fluorescence probe method. Pyrene was dissolved in acetone to form standard solution (1.0×10^{-5} M). Then, 400 μL of standard solution was added into different brown vials. Brown vials were placed in vacuum drying oven under 50°C for 30 min to make acetone evaporate completely. Blank mixed micellar solutions were diluted with deionized water to serial concentrations from 4.88×10^{-4} to 2 mg/mL and were added into brown vials to make the final pyrene concentration reach 2.0×10^{-6} M. Then, the solutions were balanced *via* ultrasound treatment for 30 min before measurement. Fluorescence spectra were measured using a fluorescence spectrometer (RF-6000;

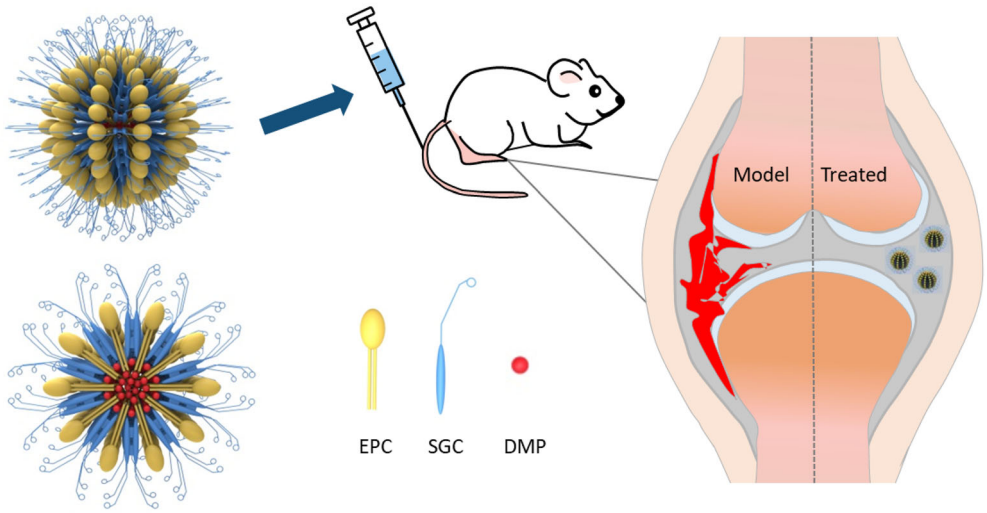

Fig. 1. Passive targeting of DMP-MMs on inflammatory joint

Shimadzu Tech, Japan). The excitation wavelength was set at 334 nm. Scanning range of emission wavelength ranges from 350 nm to 450 nm with the scanning speed of 60 nm/min. The bandwidths of excitation and emission were 5 nm and 3 nm, respectively (28).

Carrageenan-Induced Paw Edema in Rats

The preventive effect of DMP on acute inflammation was studied as previously described (29–32). Rats were administered saline or DMP-MMs (**M** 0.08, 0.16, 0.32 mg/kg) or commercially available Limethason® (L 0.16 mg/kg) *via*

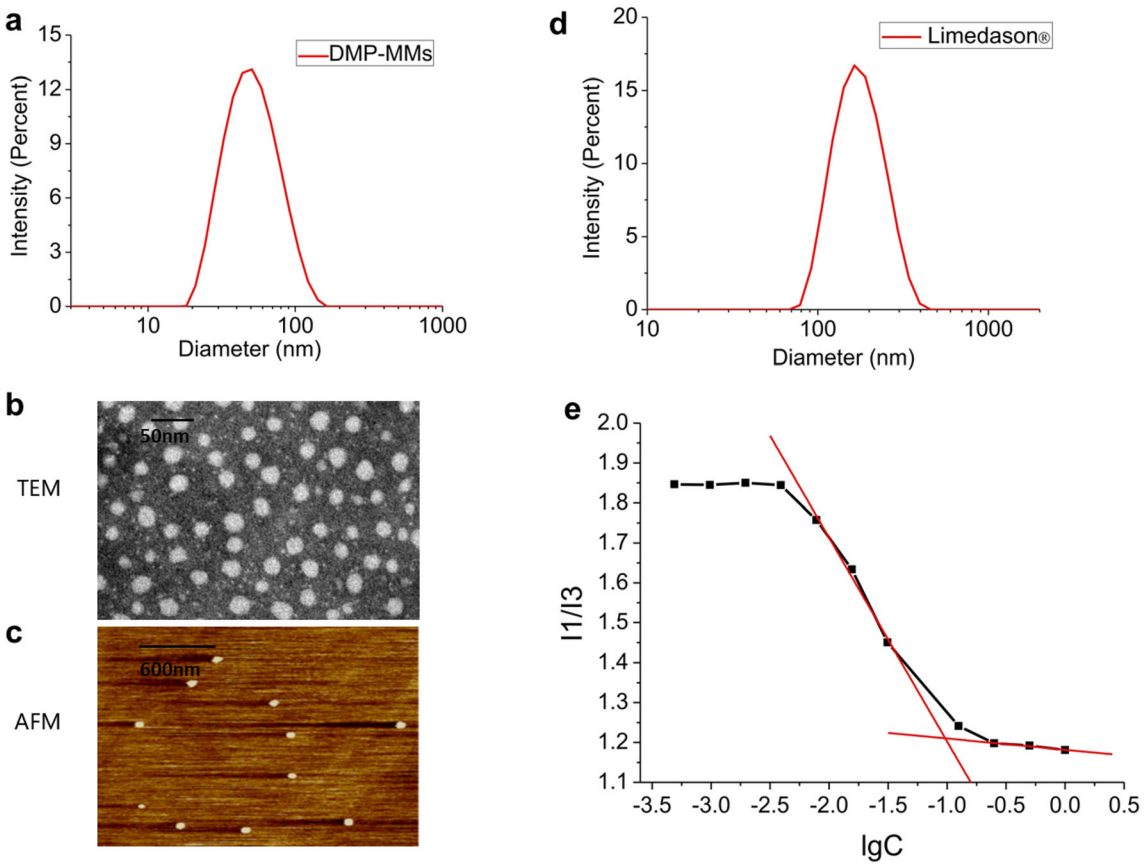

Fig. 2. Characterization of DMP-MMs. **a** Size distribution by intensity of DMP-MMs using dynamic light scattering. **b** Transmission electron microscopy of DMP-MMs. **c** Atomic force microscopy of preparation. **d** Size distribution by intensity of Limethason® using dynamic light scattering. **e** Critical micelle concentration of EYL/SGC-MMs

Table I. Encapsulation Efficiency and Drug Loading of DMP-MMs

Diameter (nm)	PDI	Zeta potential (mV)	Encapsulation efficiency (%)	Drug loading (%)
49.14 ± 0.44	0.176 + 0.013	− 33.07 ± 1.35	95.0 ± 1.6	12.8 ± 0.2

Mean ± standard deviation (SD; $n = 3$)
PDI polydispersity index, *DMP-MMs* mixed micelles loaded with dexamethasone palmitate

tail vein. After 30 min, rats were subcutaneously injected 100 μL of 1% λ-carrageenan solution into the right hind paw to induce inflammation. For evaluation of joint swelling, paw volume was measured with the plethysmometer (YSL-7C; Yiyan Tech, China) and the hind paws of rats were photographed by camera at 3 h after injecting carrageenan. At 4 h, the rats were sacrificed and plantar tissue was stripped for pathological examination of inflammation by staining with hematoxylin and eosin (H&E).

Evaluation of Anti-Arthritis Effect *In Vivo*

The CFA-induced chronic RA model was established according to other reports (33–36). SD rats were subcutaneously injected with 100 μL CFA solution into the right hind paw. At day 9, the arthritic rats were evenly divided into the test and control groups ($n = 6$) randomly. The different groups were intravenously treated as follows: saline, DMP-MMs (**M** 0.2, 0.4, 0.8 mg/kg), and Limethason® (L 0.4 mg/kg). The preparations were given every other day.

Increase in Paw Volume

The paw volume in the right hind paw was measured using the plethysmometer. The ankles were marked in each group. All the measurements were carried out by one experimenter in a blinded manner.

CT Imaging

The ankle joints of rats sacrificed at day 28 were soaked in 4% buffered paraformaldehyde for 48 h. Then we took out joints for scanning at 50 kV for 5 min (NanoSPECT/CT, Mediso, Hungary).

Histological Analysis

After the rats were sacrificed at day 28, ankle joints of rats on the right hind paw were dissected and fixed in 4% buffered paraformaldehyde for 48 h. Then, the joints were immersed in EDTA decalcifying solution at room temperature for 4 weeks. After decalcification, the joints were removed and embedded in paraffin. Then paraffin blocks

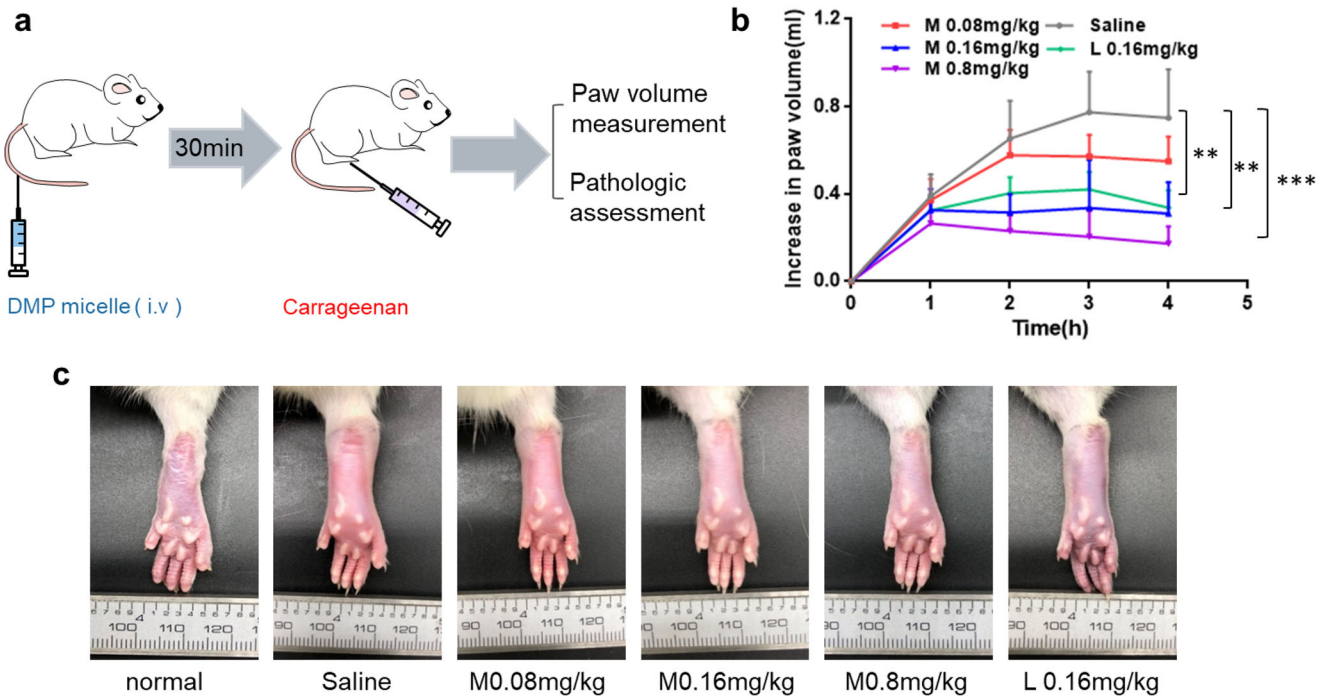

Fig. 3. Preventive effect on carrageenan-induced paw swelling. **a** Experiment process of rats study. **b** Increase in paw volume within 4 h. **c** Photographs at 3rd hour after the carrageenan administration

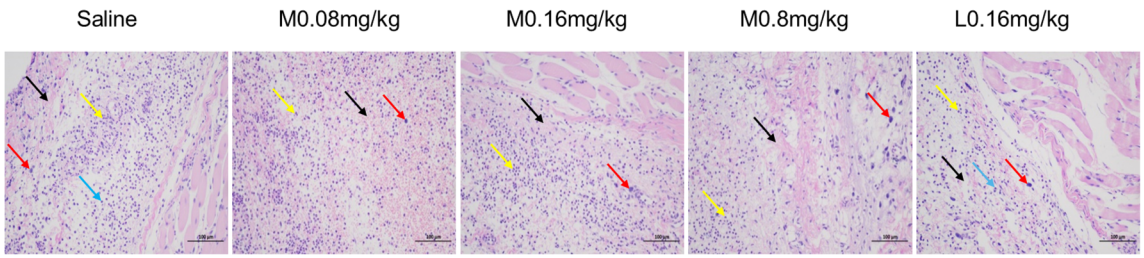

Fig. 4. H&E staining images of plantar tissue. Necrosis and dissolution of muscle fibers (black arrow), infiltration of lymphocytes (blue arrow), neutrophils (yellow arrow), and mast cells (red arrow)

were cut into sections of 4 μm. After H&E staining, the degree of joint damage was evaluated by optical microscope digital imaging system (Nikon, Japan).

Spleen index (splenic weight/rat weight) was calculated after weighing the spleen of rats. Then, the spleen was also observed pathologically according to the above steps (eliminating decalcification).

Pro-Inflammatory Cytokine Expression in Serum

Before the rats were sacrificed at day 28, blood samples were collected in the tubes. The tubes were centrifuged to separate serum samples. Final concentrations of cytokine containing TNF-α, IL-6, and IL-1β were confirmed by ELISA kits (37).

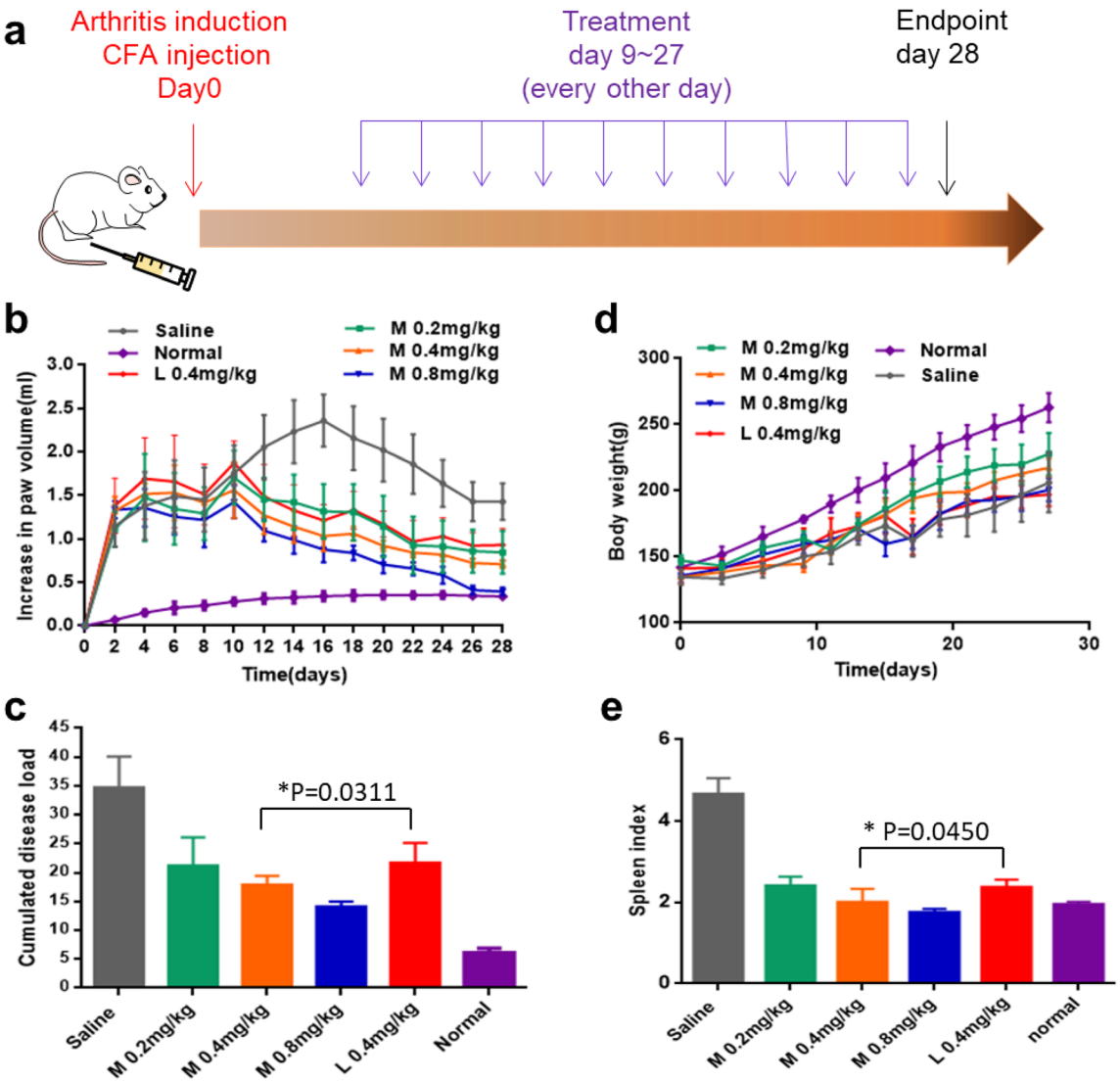

Fig. 5. DMP-MMs improved arthritic condition of rats induced by CFA. **a** Experimental scheme for model establishment and arthritic treatment. **b** Increase in paw volume from inflammation induction to the end of the experiment. **c** Cumulative disease load means the area under the curves of paw volume **b** from day 10 to day 28. **d** Body weight curves during the study. **e** Spleen index = splenic weight/rat weight

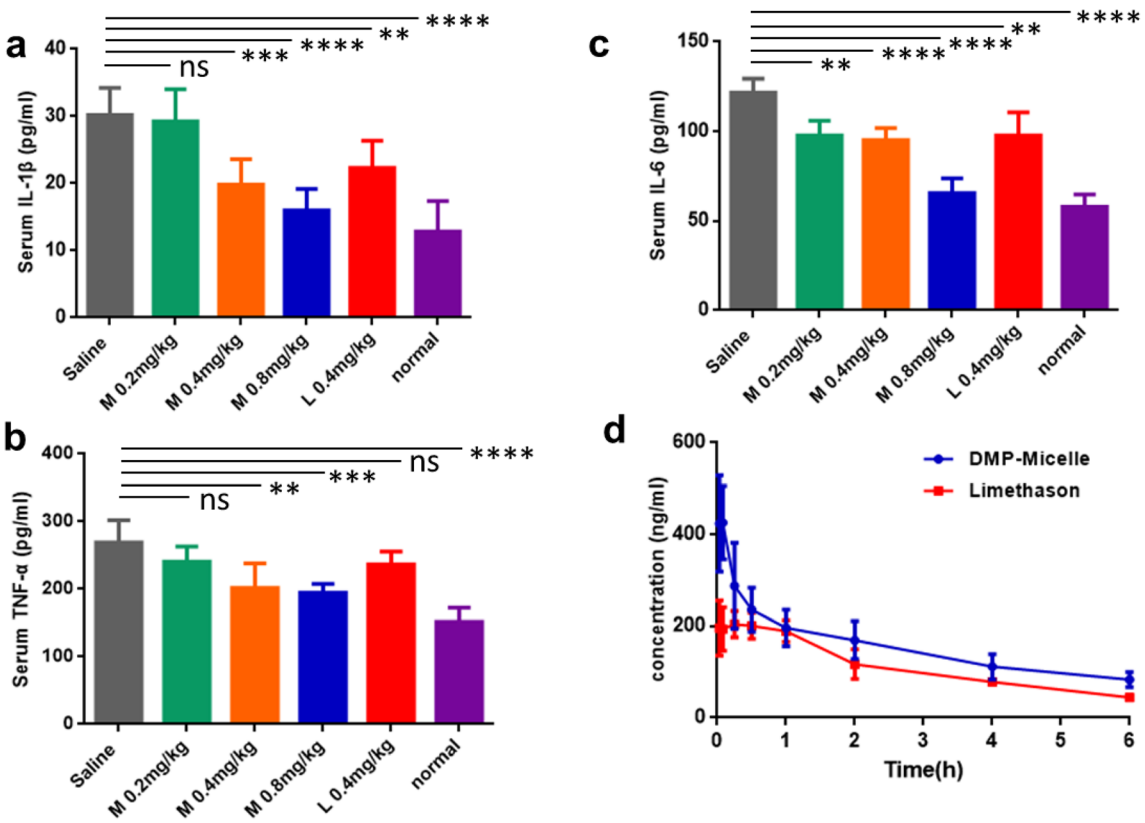

Fig.6. **a–c** The expression of pro-inflammatory cytokine in serum. **d** Plasma concentration of dexamethasone (DEX) ($n = 6$)

Biodistribution of Dir-Loaded Micelles and Emulsion

The hydrophobic fluorescent dye Dir was selected to label the nanocarriers. Free Dir solution (dissolved in 1% ethanol), Dir-MMs, and Dir-EL were intravenously injected into the rats with a swollen right hind paw. After administration, the fluorescence in rats was detected using the IVIS Spectrum system (IVIS Spectrum; Xenogen, USA) (38).

Pharmacokinetics of the DMP-MMs and Limethason® in Healthy Rats

DMP-MMs or Limethason® (1 mg/kg) were intravenously injected into the healthy male SD rats. Then, blood samples were collected and centrifuged to obtain plasma. Acetonitrile was used to extract plasma. The extracted solutions were analyzed by HPLC. Dexamethasone (DEX), an active metabolite of DMP, was detected. Pharmacokinetic parameters were analyzed by DAS2.0.

Statistical Analysis

Results were expressed as mean ± SD. Comparison of data between the two groups was done using T tests. Significant statistical differences were expressed when $P < 0.05$.

RESULTS AND DISCUSSION

Characterization of DMP-MMs

As shown in Fig. 1, the amphiphilic materials EPC and SGC self-assembled into core–shell structure. DMP, a poorly water-soluble drug, was contained in the center of mixed micelles. The results of dynamic light scattering show that the particle size of DMP-loaded micelles is approximately 49 nm with a narrow size distribution (Fig. 2a). This size of micelles provides a precondition for better targeting inflammation (39). The zeta potential was −33 mV. TEM and AFM images illustrated that DMP-MMs had a spherical structure with uniform distribution (Fig. 2b, c). Figure 2d shows the results of dynamic light scattering of Limethason®. EE% and DL% of DMP were 94.5 ± 1.4% and 12.7 ± 0.2%, respectively (Table I). The two tangent equations are $Y = -0.0283X + 1.1816$ and $Y = -0.5106X + 0.6917$ and the CMC value determined by the intersection of the tangent lines was 0.096 mg/mL (Fig. 2e).

Prophylactic Efficacy of DMP-MMs on Carrageenan-Induced Paw Edema in Rats

The experimental process is shown in Fig. 3a. The data of the paw volume show that the drug-administered groups had different degrees of inhibition on carrageenan-induced paw swelling in rats (Fig. 3b).

Photographs are displayed in Fig. 3c. In comparison to the saline treated group, both the DMP-MMs with different

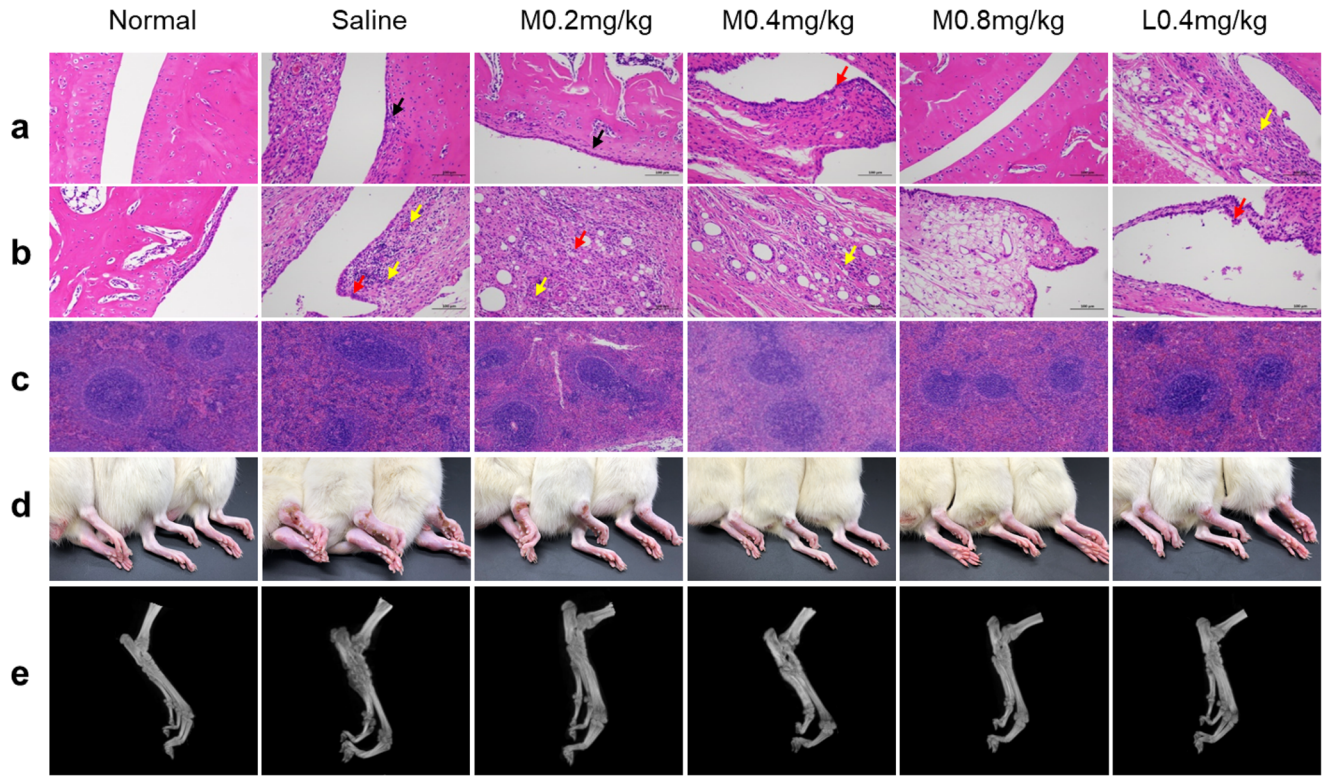

Fig. 7. DMP-MMs alleviated paw swelling and bone damage for AIA model. **a**, **b** Histopathology in ankle joints with staining reagent of hematoxylin and eosin (H&E). **c** H&E staining images of spleen. **d** Pictures of the hind paws of rats. **e** CT images of the right hind paw of rats

doses and Limethason® exhibited significant inhibition effects on carrageenan-induced paw swelling.

H&E staining images (Fig. 4) of plantar tissue illustrated that large areas of necrosis and dissolution of muscle fibers (black arrow) were observed in the saline group and Limethason® group, accompanied by a large number of lymphocytes (blue arrow), neutrophils (yellow arrow), and a small amount of mast cell (red arrow) infiltration. Yet, the amount of inflammatory cells in the Limethason® group was less than the saline group. The degree of inflammation in the middle and high-dose groups of DMP-MMs also decreased.

Therapeutic Efficacy of DMP-MMs on CFA-Induced Chronic Inflammation in Rats

The AIA model is a classical animal model to study RA. Studies have shown that AIA model is easy to establish and has many similarities with human RA in clinical manifestations, pathology, and immunology. Therefore, AIA model is widely used in RA-related research (40). The inflammatory response in rats is divided into acute phase and chronic phase (41). One day after induction of inflammation, acute local inflammatory reaction appeared and gradually decreased after 3 days. Secondary lesions usually appeared from 11 to 14 days after inflammation (42). They were characterized by multiple arthritis, accompanied by inconvenient movement, nasal congestion, redness and swelling of bilateral ear, and nodules in the tail of rats.

Table II. Key Pharmacokinetic Parameters

	AUC_{0-t} (μg/l*h)	$T_{1/2}$ (h)	C_{max} (μg/l)
DMP-MMs	1047.78 ± 98.92****	2.93 ± 0.91	472.51 ± 66.40****
Limethason®	681.19 ± 84.62	2.48 ± 0.25	238.09 ± 33.10

**** represent significant differences ($P < 0.0001$) between micelles and emulsion groups, which was calculated by the T test using GraphPad
Mean ± standard deviation (SD; $n = 6$)
AUC area under the concentration–time curve, $T_{1/2}$ half-life, C_{max} the maximum concentration of dexamethasone in plasma, *DMP-MMs* mixed micelles loaded with dexamethasone palmitate

As shown in Fig. 5a, rats were injected with CFA to induce RA at day 0, and treated with saline, DMP-MMs, and Limethason® from the 9th day.

Paw volume is a crucial index for evaluating anti-inflammatory effect. Figure 5b shows an increase in paw volume of DMP-MMs, Limethason®, and the control group. The degree of paw swelling obviously decreased in all drug-treated groups from days 12 to 28. The improvement of anti-inflammatory activity could be further explained by cumulated disease load. As shown in Fig. 5c, the cumulated disease load between the DMP-MMs and Limethason® group with 0.4 mg/kg was significantly different ($P < 0.05$).

The weight curves of rats within 28 days are displayed in Fig. 5d. Compared with normal rats, the body weight in saline group decreased remarkably when inflammation appeared ($P < 0.01$). The body weight in Limethason® group was remarkably lower than DMP-MMs group ($P < 0.05$) from 15th day to the end.

As shown in Fig. 5e, the spleen index shows significant difference ($P < 0.05$) between DMP-MMs group and

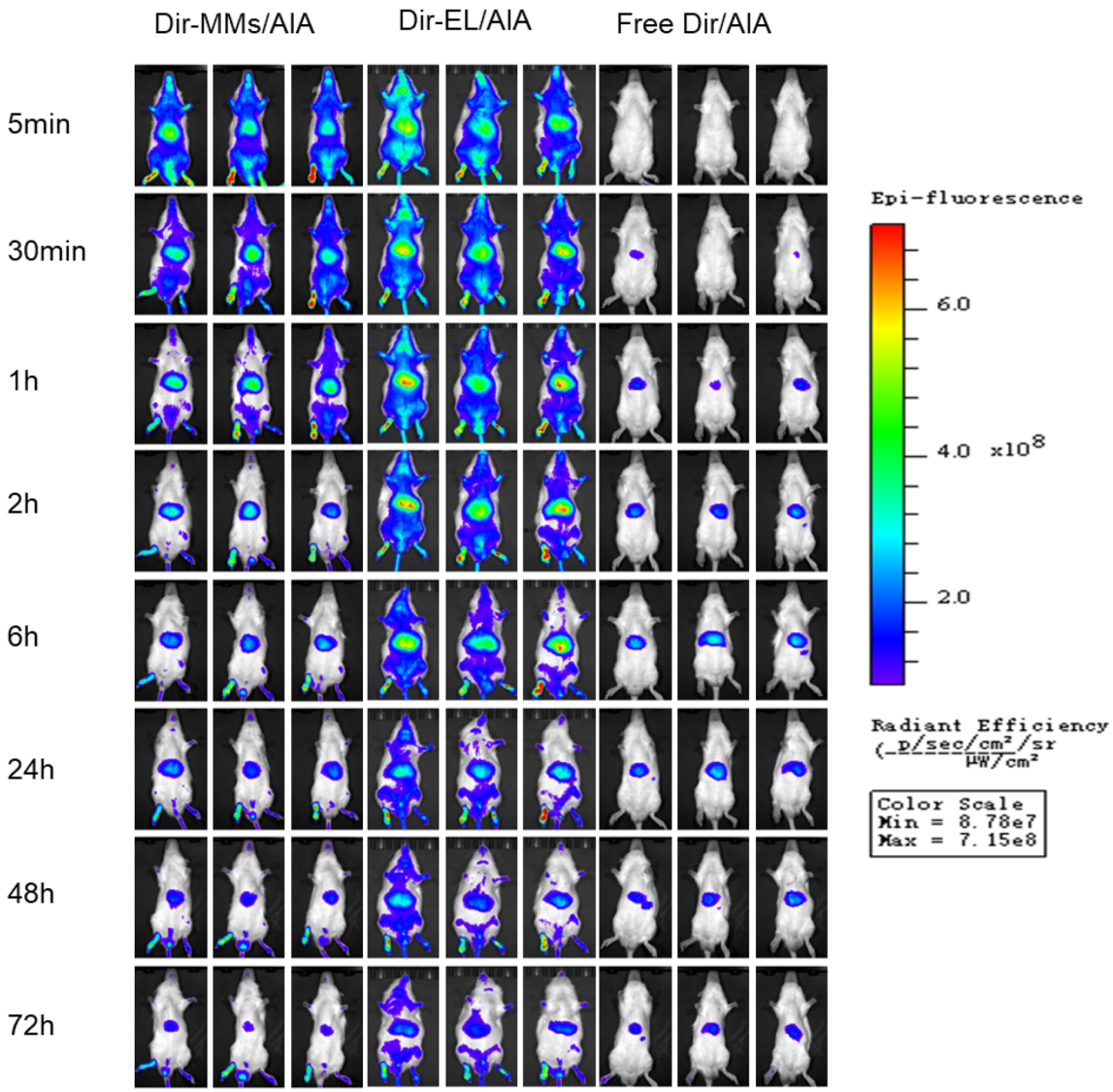

Fig. 8. Fluorescent images after intravenous injecting different Dir preparations ($n = 3$)

Limethason® group with the dose of 0.4 mg/kg. The spleen structure of the normal group was intact, and the spleen morphological structure was clear, and the boundary with the red pulp was obvious (Fig. 7c). In the model group, the morphology of splenic corpuscles was abnormal, and germinal centers began to appear. The erythrocyte in red pulp increased with congestion and inflammatory cell infiltration. For the drug treatment groups, the pathological changes of spleen in AIA rats were improved in different extent.

Pro-inflammatory cytokines were key parameters for evaluating therapeutic effect. The serum levels of three cytokines in the saline group were evidently upregulated in comparison to the normal group. The concentration of cytokines in DMP-MMs groups showed dose-dependent downregulation. Especially in medium and high-dose groups, the reduction of inflammatory factors was significant compared with saline group (Fig. 6a–c).

H&E photographs of the ankle joints show inflammatory cell infiltration on the surface of articular cartilage (black arrow), synovial cell lining hyperplasia (red arrow), synovial connective tissue hyperplasia, accompanied by inflammatory cell infiltration, and visible vasospasm (yellow arrow) in CFA model group (Fig. 7a, b). Articular cartilage surface is smooth and flat; no obvious hyperplasia and other changes in synovial membrane were observed in the DMP-MM high-dose group. The remaining drug-administered groups had different degrees of relief.

Pictures in Fig. 7d show that the rats of the saline-treated group had swollen hind paws. Also, fester symptoms appeared in the paw injected with CFA. However, the high-dose administration of DMP-MMs (0.8 mg/kg) completely prevented the progression of arthritis. DMP-MMs and Limethason® groups with 0.4 mg/kg both significantly alleviated paw swelling of rats. A lower dose of DMP-MMs (0.2 mg/kg) had a slight therapeutic effect.

Figure 7e shows the CT scanning images of the ankle joints in each group. For saline group, swelling of ankle joint and soft tissue, narrowing of joint space, osteoporosis at the end of bone, and deformity of the distal interphalangeal joint appeared. For treated groups, there was no obvious metamorphosis of the joints, but there was mild osteoporosis in the proximal joint.

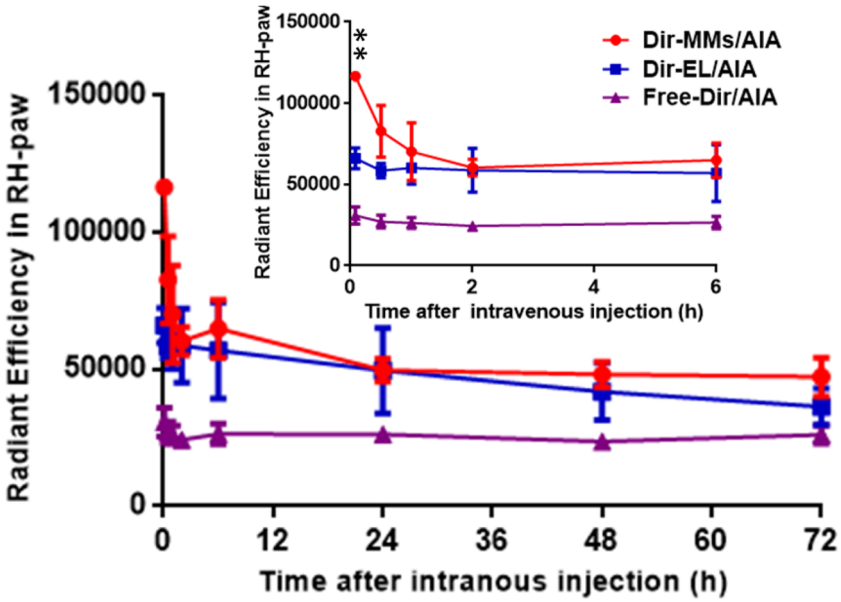

Fig. 9. Relative fluorescence intensity measured in the right hind paw (RH-paw) in each rat. $^{**}P < 0.001$ indicates significant difference between Dir-MMs and Dir-EL at 5 min ($n = 3$)

Pharmacokinetics of DMP-MMs and Limethason®

The pharmacokinetic results are shown in Fig. 6d and Table II. The concentration of DEX was used to study the dynamic changes of DMP-MMs and Limethason® *in vivo*. As shown in Table II, DMP-MM group was significantly higher than Limethason® group in the aspects of AUC_{0-t} ($P < 0.0001$) and C_{max} ($P < 0.0001$). This result explains the superior anti-inflammatory effects of the DMP-MMs to some extent.

Biodistribution of Dir-Loaded Micelles and Emulsion

Using the Dir-labeled micelles and emulsions, the fluorescence strength difference between the injured right paw and the healthy left paw reflected the selective accumulation of different preparations in the inflammatory sites. Meantime, the DMP-MMs exhibited significantly higher enrichment in the CFA-treated right paw than Limethason®. Radioactive-labeled liposomes below 100 nm have been successfully used for imaging and detecting inflammatory sites in animal models and humans (43–45). The superior targeting ability of the DMP-MMs explains its better anti-inflammatory effects.

Figure 8a displays the fluorescence images of different Dir preparations in AIA rats. The fluorescence intensity of the Dir-MMs was stronger than that of the Dir-EL in the inflammatory paw (Fig. 8b). What is more, the difference was highly significant at the time point of 5 min ($P < 0.01$). Free Dir rarely distributed in the inflamed paw (Fig. 9).

CONCLUSION

Mixed micelles encapsulated with DMP were prepared by a simple and mature process. It is well known that lecithin and bile salts are important physiological substances in the normal human body. Also, the egg yolk lecithin in the prescription is an injection-grade pharmaceutical excipient with high safety. In addition, micelles exhibited higher bioavailability and passive targeting of inflammatory sites in this research. Therefore, it has guiding significance for the clinical treatment of inflammatory diseases, and it is promising for industrial production.

ACKNOWLEDGMENTS

We thank Beijing Delivery Pharmaceutical Technology Co., Ltd. for supporting Limethason® and NaOH. We would like to thank members of our laboratory for their help and support.

REFERENCES

1. Smolen JS, Aletaha D, Mcinnes IB. Rheumatoid arthritis. Lancet. 2016;388(10055):2023–38.
2. Lee SM, Kim HJ, Ha YJ, Park YN, Lee SK, Park YB, et al. Targeted chemo-photothermal treatments of rheumatoid arthritis using gold half-shell multifunctional nanoparticles. ACS Nano. 2013;7(1):50–7.
3. Bathon JM, Moreland LW, Dibartolomeo AG. Inflammatory central nervous system involvement in rheumatoid arthritis. Semin Arthritis Rheum. 1989;18(4):258–66.
4. Takeuchi O, Akira S. Pattern recognition receptors and inflammation. Cell. 2010;140(6):805–20.
5. Hoes JN, Jacobs JWG, Buttgereit F, Bijlsma JWJ. Current view of glucocorticoid co-therapy with DMARDs in rheumatoid arthritis. Nat Rev Rheumatol. 2010;6(12):693–702.
6. Singh JA, Saag KG, Bridges SL Jr, Akl EA, Bannuru RR, Sullivan MC. 2015 American College of Rheumatology Guideline for the treatment of rheumatoid arthritis. Arthritis Rheumatol. 2016;68(1):1–26.
7. Yuan F, Quan LD, Cui L, Goldring SR, Wang D. Development of macromolecular prodrug for rheumatoid arthritis. Adv Drug Deliv Rev. 2012;64(12):1205–19.

8. Baschant U, Lane NE, Tuckermann J. The multiple facets of glucocorticoid action in rheumatoid arthritis. Nat Rev Rheumatol. 2012;8(11):645–55.
9. Bevaart L, Vervoordeldonk MJ, Tak PP. Evaluation of therapeutic targets in animal models of arthritis: how does it relate to rheumatoid arthritis? Arthritis Rheum. 2010;62(8):2192–205.
10. Marco K, Christoph B. The current relevance and use of prednisone in rheumatoid arthritis. Expert Rev Clin Immunol. 2014;10(5):557–71.
11. Matsumura YM, Maeda HA. A new concept for macromolecular therapeutics in cancer chemotherapy: mechanism of tumoritropic accumulation of proteins and the antitumor agent smancs. Cancer Res. 1986;46(12 **Pt 1**):6387–92.
12. Jia M , Deng C , Luo J , Zhang P, Sun X,Zhang Z, Gong T. A novel dexamethasone-loaded liposome alleviates rheumatoid arthritis in rats. Int J Pharm 2018;540(1–2):57–64.
13. Zhenshan J, Xiaobei W, Xin W, Gang Z, Foster KW, Fang Q, et al. Micelle-forming dexamethasone prodrug attenuates nephritis in lupus-prone mice without apparent glucocorticoid side effects. ACS Nano. 2018;12(8):7663–81.
14. Bahadori F, Topçu G, Eroğlu MS, Önyüksel H. A new lipid-based nano formulation of vinorelbine. AAPS PharmSciTech 2014;15:1138, 1148.
15. Durymanov M, Kamaletdinova T, Lehmann SE, Reineke J. Exploiting passive nanomedicine accumulation at sites of enhanced vascular permeability for non-cancerous applications. J Control Release. 2017;261:10–22.
16. Yang M, Feng X, Ding J, Chang F, Chen X. Nanotherapeutics relieve rheumatoid arthritis. J Control Release. 2017;252:108–24.
17. Prasad LK, O'Mary H, Cui Z. Nanomedicine delivers promising treatments for rheumatoid arthritis. Nanomedicine. 2015;10(13):2063–74.
18. Lingdong Q, Yijia Z, Bart J. Crielaard, Anand Dusad, Subodh M. Lele, Cristianne JF, Rijcken et al. Nanomedicines for inflammatory arthritis: head-to-head comparison of glucocorticoid-containing polymers, micelles, and liposomes. ACS Nano 2014; 8(1):458–466.
19. Pradip N, Gajanand S, Bhupinder S, Khuller GK, Goni VG, Patil AB, et al. Preclinical explorative assessment of celecoxib-based biocompatible lipidic nanocarriers for the management of CFA-induced rheumatoid arthritis in Wistar rats. AAPS PharmSciTech. 2018;19(7):3187–98.
20. Javed I, Hussain SZ, Ullah I, Khan I, Ateeq M, Shahnaz G, et al. Synthesis, characterization and evaluation of lecithin-based nanocarriers for the enhanced pharmacological and oral pharmacokinetic profile of amphotericin B. J Mater Chem B. 2015;3:8359–65.
21. Javed I, Hussain SZ, Shahzad A, Khan JM, Habibur-Rehman MR, et al. Lecithin-gold hybrid nanocarriers as efficient and pH selective vehicles for oral delivery of diacerein—in-vitro and in-vivo study. Colloids Surf B: Biointerfaces. 2016;141:1–9.
22. Mitragotri S, Yoo JW. Designing micro- and nano-particles for treating rheumatoid arthritis. Arch Pharm Res. 2011;34(11):1887–97.
23. Dong F, Xie Y, Qi J, Hu F, Lu Y, Li S, et al. Bile salt/phospholipid mixed micelle precursor pellets prepared by fluid-bed coating. Int J Nanomedicine. 2013:1653–63.
24. Chopra P, Hao J, Li SK. Influence of drug lipophilicity on drug release from sclera after iontophoretic delivery of mixed micellar carrier system to human sclera. J Pharm Sci. 2013;102(2):480–8.
25. Yokoyama K, Watanabe M. Limethason as a lipid microsphere preparation: an overview. Adv Drug Deliv Rev. 1996;20(2):195–201.
26. Duan Y, Wang J, Yang X, Du H, Zhai G. Curcumin-loaded mixed micelles: preparation, optimization, physicochemical properties and cytotoxicity in vitro. Drug Deliv. 2014;22(1):50–7.
27. Seki J, Sonoke S, Saheki A, Fukui H, Sasaki H, Mayumi T. A nanometer lipid emulsion, lipid nano-sphere (LNS), as a parenteral drug carrier for passive drug targeting. Int J Pharm. 2004;273(1–2):75–83.
28. Liu Z, Chen M, Guo Y, Wang X, Zhang L, Zhou J, et al. Self-assembly of cationic amphiphilic cellulose-g-poly (p-dioxanone) copolymers. Carbohydr Polym. 2019;204:214–22.
29. Jiang Z, Zhao C, Gong X, Sun X, Li H, Zhao Y, et al. Quantification and efficient discovery of quality control markers for, Emilia prenanthoidea, DC. by fingerprint–efficacy relationship modelling. J Pharm Biomed Anal. 2018;156:36–44.
30. Chen Y, Yu H, Guo F, Wu Y, Li Y. Antinociceptive and anti-inflammatory activities of a standardized extract of bis-iridoids from Pterocephalus hookeri. J Ethnopharmacol. 2018;216:233–8.
31. Muhammad M, Bakht N, Saniya ZS, Rashid KM, Bushra M, Ihsan-Ul H. Ipomoea batatas L. Lam. ameliorates acute and chronic inflammations by suppressing inflammatory mediators, a comprehensive exploration using in vitro and in vivo models. BMC Complementary and Altern Med. 2018;18(1):216.
32. Boughton-Smith NK, Deakin AM, Follenfant RL, Whittle BJR, Garland LG. Role of oxygen radicals and arachidonic acid metabolites in the reverse passive Arthus reaction and carrageenin paw oedema in the rat. Br J Pharmacol. 1993;110(2):896–902.
33. Buritova J, Honoré P, Chapman V, Besson JM. Enhanced effects of co-administered dexamethasone and diclofenac on inflammatory pain processing and associated spinal c-Fos expression in the rat. Pain. 1996;64(3):559–68.
34. Laste G, Ripoll Rozisky J, De Macedo IC, Vinicius SDS, de Souza C, Cristina I, et al. Spinal cord brain-derived neurotrophic factor levels increase after dexamethasone treatment in male rats with chronic inflammation. Neuroimmunomodulation. 2013;20(2):119–25.
35. El-Rahman RSA, Suddek GM, Gameil NM, El-Kashef HA. Protective potential of MMR vaccine against complete Freund's adjuvant-induced inflammation in rats. Inflammopharmacology. 2011;19(6):343–8.
36. Khaled KA, Sarhan HA, Ibrahim MA, Ali AH, Naguib YW. Prednisolone-loaded PLGA microspheres. In vitro characterization and in vivo application in adjuvant-induced arthritis in mice. AAPS PharmSciTech. 2010;11(2):859–69.
37. Li XY, Li H, Zhang Y, Gao S, Dong CP, Wu GF. Development of albumin coupled, cholesterol stabilized, lipid nanoemulsion of methotrexate, and TNF-α inhibitor for improved in vivo efficacy against rheumatoid arthritis. AAPS PharmSciTech. 2017;18(7):2774–82.
38. Lianghui Y, Peng B, Dong C, Liuli X, Kam WL, Chenyong M. A KALA-modified lipid nanoparticle containing CpG-free plasmid DNA as a potential DNA vaccine carrier for antigen presentation and as an immune-stimulative adjuvant. Nucleic Acids Res. 2015;43(3):1317–31.
39. Crielaard BJ, Lammers T, Schiffelers RM, Storm G. Drug targeting systems for inflammatory disease: one for all, all for one. J Control Release. 2012;161(2):225–34.
40. Wei F, Xu S, Jia X, Sun X, Chang Y. BAFF and its receptors involved in the inflammation progress in adjuvant induced arthritis rats. Int Immunopharmacol. 2016;31:1–8.
41. Bernardi A, Zilberstein AE JÃºg, Campos MM, Morrone FB, Calixto JB, et al. Effects of indomethacin-loaded nanocapsules in experimental models of inflammation in rats. Br J Pharmacol. 2009;158(4):1104–11.
42. Ben IO, Woode E, Koffuor GA, Boakyegyasi E, Titiloye NA. Effects of Trichilia monadelpha (Meliaceae) extracts on bone histomorphology in complete Freund's adjuvant-induced arthritis. J Intercult Ethnopharmacol. 2017;6(2):177–85.
43. Dams ETM, Reijnen MMPJ, Oyen WJG, Boerman OC, Laverman P, Storm G, et al. Imaging experimental intraabdominal abscesses with 99mTc-PEG liposomes and 99mTc-HYNIC IgG. Ann Surg. 1999;229(4):551–7.
44. Laverman P, Dams ETM, Oyen WJG, Storm G, Koenders EB, Prevost R, et al. A novel method to label liposomes with Tc-99m by the hydrazino nicotinyl derivative. J Nucl Med. 1999;40(1):192–7.
45. Boerman O, Oyen W, Storm G, Corvo M, van Bloois L, van der Meer JWM, et al. Technetium-99m labeled liposomes to image experimental arthritis. Ann Rheum Dis. 1997;56(6):369–73.